archives
of thermodynamics
Vol. **42**(2021), No. 4, 201–216
DOI: 10.24425/ather.2021.139659

Application of overset mesh approach in the investigation of the Savonius wind turbines with rigid and deformable blades

EMIL MARCHEWKA*
KRZYSZTOF SOBCZAK
PIOTR REOROWICZ
DAMIAN STANISŁAW OBIDOWSKI
KRZYSZTOF JÓŹWIK

Lodz University of Technology, Institute of Turbomachinery,
Wólczańska 219/223, 90-924 Łódź, Poland

Abstract Machines utilising renewable energy constantly undergo research aimed at raising their efficiency. One of them is a Savonius wind turbine, where scientists propose adjustments to improve its aerodynamic properties. At present, their assessment is usually performed by means of transient computational fluid dynamics simulations with two- or three-dimensional models. In this paper, the overset (chimera) mesh approach was applied to investigate the performance of a Savonius wind turbine equipped with deformable blades. They were continuously deformed during rotation by a dedicated mechanism to increase a positive torque of the advancing blade, and meanwhile, decrease a negative torque of the returning blade. A quasi-two-dimensional model with a two-way fluid-structure interaction method was applied, where the structural solver determined blade deflection caused by the predefined deformation mechanism and aerodynamic loads, whereas the coupled computational fluid dynamics solver determined the transient flow. The deformable blades rotor performance was calculated and compared with a conventional rigid Savonius turbine, both simulated using the overset mesh approach. The average value of the power coefficient achieved a 55% rise in the case of deformable blades turbine. Additionally, to validate the overset method, its results were compared with the classical sliding mesh method for a conventional rigid rotor.

Keywords: CFD; Savonius; Deformable blade; Overset mesh; Sliding mesh

*Corresponding Author. Email: emil.marchewka@dokt.p.lodz.pl

Nomenclature

C_p	–	power coefficient
C_t	–	torque coefficient
D	–	turbine diameter, m
e	–	blade overlap, m
FGCI	–	fine-grid convergence index
H	–	turbine section height, m
m	–	displacement of rotation axis, m
P	–	apparent order of the method
R	–	error ratio
RE	–	extrapolated value
T	–	torque, Nm
TSR	–	tip speed ratio
t	–	turbine blade thickness, mm
U	–	wind velocity, m/s
y^+	–	non-dimensional wall distance

Greek symbols

ρ	–	air density, kg/m^3
ω	–	turbine angular velocity, rad/s

Acronyms

CFD	–	computational fluid dynamics
FSI	–	fluid-structure interaction
HAWT	–	horizontal axis wind turbine
VAWT	–	vertical axis wind turbine

1 Introduction

A constant search for relatively simple and versatile green energy sources implies the creation of innovative designs and further development of already existing machines. In a wind energy field, one of the trends is the development of small wind turbines for domestic or micro-grid applications. One of the devices subjected to the research and development process is the Savonius wind turbine. It is a vertical axis wind turbine (VAWT) that operates independently of the wind direction. In comparison to conventional horizontal axis wind turbines (HAWTs), it starts at lower wind speeds but suffers from a lower efficiency [1]. Contemporary development works concentrate on raising its efficiency by modification of blade geometry [2,3], or application of shielding elements and ducts [4–6]. Our concept aims at the application of deformable blades [7,8].

The traditional approach of aerodynamic performance evaluation of new ideas requires time and resource-demanding manufacturing of turbine mod-

els and testing them in wind tunnels [9,10]. Therefore, computational fluid dynamics (CFD) simulations are useful for fast and cheap verification of developed concepts [11–13]. Usually, computational models of Savonius turbines apply a sliding mesh approach, where the flow domain contains two non-overlapping regions and an interface exchanging solution data between them [12–15]. The internal circular region contains the rotor with the adjacent surrounding environment and rotates with specified angular velocity. The external stationary one represents the further turbine surroundings. The method serves well for fixed geometry turbines. However, its application to the rotor with deformable elastic blades is difficult, as the internal mesh requires deforming and remeshing in the subsequent time steps [7].

For such cases, the overset mesh method is a solution to simplify the computational model. This approach requires independent overlapping meshes for the background computational domain and the adjacent surroundings of the solid bodies placed in the flow (overset meshes). The solver automatically creates a data interface between the background and boundaries of overset meshes. Then, donor and receptor cells are chosen to interpolate and pass the data between them to obtain the background mesh locally merged with overset meshes [16]. In this scenario, the quality of each overset mesh as well as their movement, deflection and remeshing can be controlled independently of the remaining ones before the merging process. Additionally, applied overset meshes can be of more complex contours than circular as in the sliding mesh method.

The paper presents the overset mesh method applied to assess the aerodynamic performance of a Savonius wind turbine with deformable overlapped blades. They were continuously deformed during rotation by a dedicated mechanism to enhance generated torque. The developed computational model was used to analyse the performance of a reference fixed geometry Savonius turbine of comparable size to judge the performance gain of the deformable blades. The reference machine was also investigated with a conventional sliding mesh computational model to provide a comparison of solutions obtained by both methods.

2 Methodology

Three task configurations were solved. The computational models utilising overset approach were used to compare the performance of the turbine with deformable blades and its rigid equivalent. The blade deformation was pro-

vided by combining the fluid flow and the structural simulations. Additionally, the traditional sliding mesh simulation of the rigid blades turbine was made for comparison with the overset method. A full 3D simulation of the deformable turbine was not possible due to enormous requirements for the computational power of both the fluid flow and structural solvers. Hence, the performance of the presented turbines was investigated through the quasi-2D transient models in Ansys Workbench 2020 R2 [17] containing the Ansys Fluent fluid flow solver and the Ansys Transient Structural solver. Limitations of the latter one rejected the creation of a fully 2D model. The blade deformation determined in the structural solver was transferred to the flow solver and the aerodynamic loads at walls were transferred back to the structural solver using a two-way fluid-structure interaction (FSI) coupling.

The reference turbine rotor subjected to investigations was a Savonius type with semi-circular blades. It had the diameter $D = 1$ m with the overlap between the blades $e = 0.1$ m and the blade thickness $t = 1$ mm. Its exemplary design is shown in Fig. 1a. The prototype utilising deformable

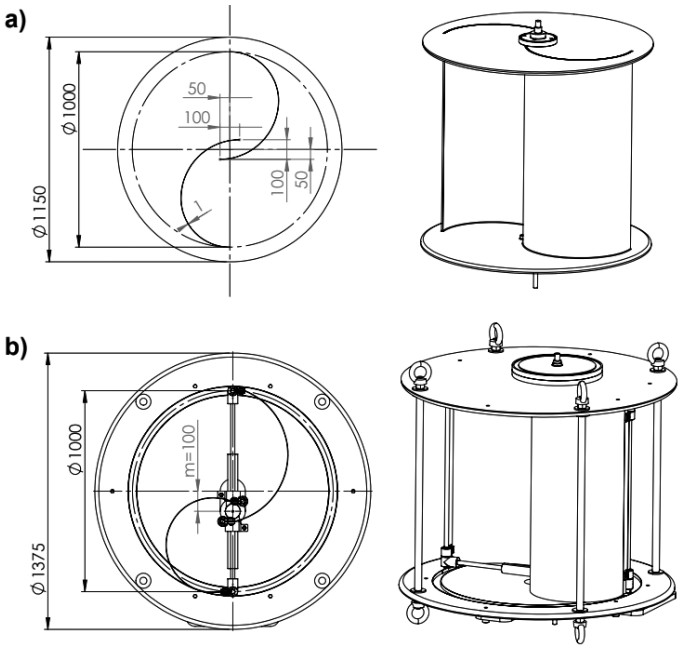

Figure 1: a) Conventional Savonius turbine with indicated basic dimensions. b) Savonius turbine with deformable blades with the same diameter and overlap and the rotation axis eccentricity of 10%.

blades was of the same diameter and overlap, but the rotation axis of blades was moved by $m = 0.1$ m ($m/D = 10\%$ of eccentricity) from the turbine centre (Fig. 1b). The deforming mechanism utilised the eccentric rotation axis to continuously alter frontal areas of the advancing and returning blades and, thus, increase the torque generated by the turbine. Its design and operation principle was thoroughly explained in [7, 8].

2.1 Fluid flow model definition

The turbines' sections were investigated inside the flow domains of dimensions 25 m by 20 m which limited the blockage effect. Due to the quasi-2D approach, the domain thickness was 5 mm and elements of the blade deforming mechanism were omitted as they influence the airflow only at the top and bottom regions of the rotor. The boundary of overset meshes was offset 60 mm from the turbine blades. In the case of the sliding mesh simulation, the inner domain diameter was 1.5 m. Detailed dimensions and location of the turbine rotor section in an initial position are shown in Fig. 2.

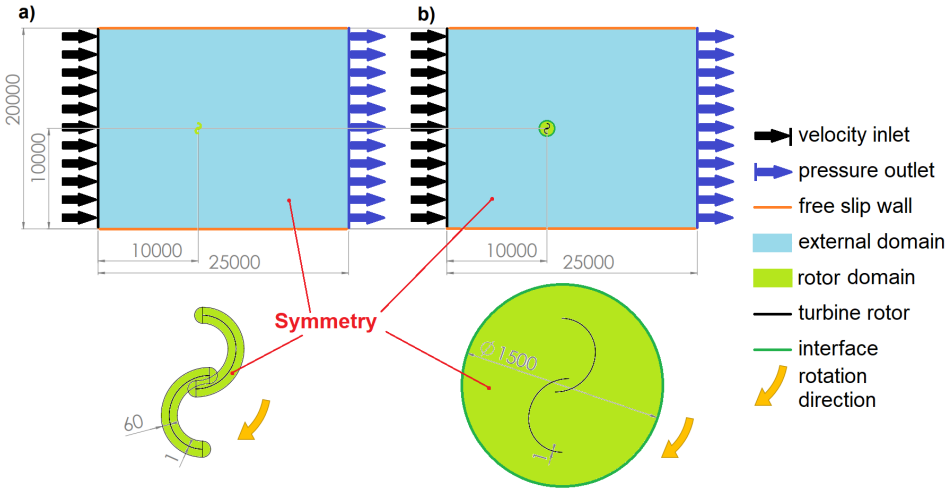

Figure 2: Overset a) and sliding mesh domains b) with magnified rotor surroundings (dimensions in mm).

In all cases, one layer of hexahedral unstructured mesh was used. In the case of the overset approach, the edge size of elements was 4 mm for the overlapping mesh and the background mesh at the region covered by the rotor diameter. The same element size was used in the inner rotating region in

the case of the sliding mesh approach. Additional meshes with element edge sizes equal to 6 and 8 mm were also created to estimate the discretization uncertainty. In all cases beyond the rotor region, the elements gradually increased up to 100 mm at domain borders with a 1.05 growth rate. The region of the blade vicinity was defined in the same way for the overlapping meshes in the overset method and the sliding mesh method. The local refinement up to 0.025 mm at the blade tips was applied. The inflation layer was used at blade walls. The height of the first layer was 0.05 mm, which allowed for obtaining $y^+ < 1$ (non-dimensional wall distance) and full solution of the boundary layer in the vast majority of blade areas during all rotation phases. Detailed views of both meshes in the blade vicinity are shown in Fig. 3.

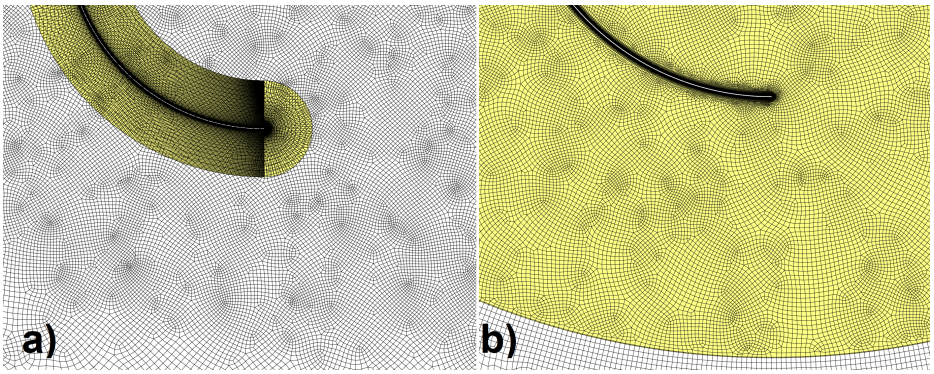

Figure 3: A close-up on meshes of rotor surrounding and background: a) overset mesh, b) sliding mesh.

In all cases, the transient simulations were carried out with the Reynolds averaged Navier–Stokes (RANS) pressure-based solver of Ansys Fluent. The k-ω SST (shear stress transport) turbulence model of Menter [18] was applied. Due to its good performance in the flows with the adverse pressure gradient and separations, it was successfully used in simulations of the Savonius turbines [19–23]. Air was treated as compressible with its properties defined for standard atmospheric conditions (1 atm and 15°). The air velocity at the inlet was equal to 4 m/s which corresponded to the Reynolds number based on turbine diameter equal to 2.7×10^5. Additionally, the turbulence intensity of 5% and the viscosity ratio of 10 were specified. At the outlet of the domain, the atmospheric pressure was applied. At the turbine blades, the no-slip and smooth wall boundary conditions were defined. No shear wall condition was used at the top and bottom of the domains.

Following the quasi-2D approach, the symmetry condition was defined at two sides of the mesh slice (Fig. 2). The overset meshes were defined as deformable, with the use of a smoothing algorithm based on the spring method to preserve a good quality of the thinnest elements of the inflation layer.

The overset meshes around blades in the overset method and the inner mesh region in the sliding mesh method revolved clockwise with the angular velocity $\omega = 6.4$ rad/s (61.15 rpm), which corresponded to tip speed ratio of 0.8,

$$\mathrm{TSR} = \frac{\omega D}{2U}\,. \tag{1}$$

Appropriate interfaces passing data between meshes in the rotating and stationary frames of references were defined for both methods.

The Coupled pressure-velocity coupling method was used with the second-order spatial discretization schemes for mass, momentum and energy equations as well as for the turbulence model transport equations. The first-order implicit transient scheme was used. 1080 time steps were solved for one revolution of the rotor. In every case, at least 15 full revolutions were solved to obtain a stabilised flow. Each time step of the transient simulation was solved maximally within 100 iterations, however, in the vast majority of time steps, the residual target of 10^{-3} was reached for all equations in less than 30 iterations. Only a few time steps did not achieve the criterion due to random numerical instabilities resulting from mesh deformation and interpolation of data between distant cells in the overset approach.

2.2 Structural model definition

The quasi-2D structural modelling of the blade deforming mechanism shown in Fig. 4 was carried out in the Ansys Structural solver. The model was 5 mm thick with one layer of unstructured hexahedral elements. Blades (a) consisted of two layers of 0.5 mm elements. The guiding ring (b), being the endplate track (Fig. 1b), consisted of 7 mm edge size elements. Two sliders (c) were meshed mainly with 10 mm elements, while 3 mm elements covered ends where blade tips were anchored. The remaining hub (d) was defined as rigid and excluded from meshing and structural analysis to reduce model complexity. The red dot (e) indicated the turbine (guiding ring) centre, while the green one (f) was the blades (rotor) rotation axis.

Applied material properties were taken from the standard Ansys library. The blades were assigned with 316 steel with Young's modulus equal to

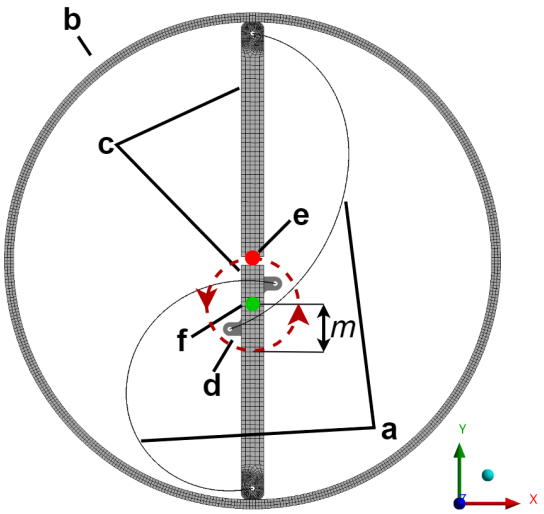

Figure 4: Deforming mechanism with implemented eccentricity: a – blades, b – guiding ring, c – sliders, d – hub, e – turbine central axis and its trajectory, f – turbine rotation axis.

195 GPa and Poisson's ratio of 0.27. Its tensile ultimate and yield strengths were 565.1 MPa and 252.1 MPa, respectively. Structural steel with Young's modulus of 200 GPa and 0.30 Poisson's ratio was applied to the remaining elements. Its tensile ultimate strength was 460 MPa and yield strength was 250 MPa.

The deformation of turbine blades was caused by the interaction of the sliders and the guiding ring. The two-way FSI coupling method in Ansys Workbench allowed for the definition of the rotational motion between structural and fluid flow solvers. Therefore, to simplify the structural model definition and analysis, the blades and sliders were solved in the stationary frame of reference, whereas the guiding ring rotated eccentrically in the counter-clockwise direction. Then, during the data transfer to the fluid flow solver, the specified angular velocity was added to provide the appropriate blade motion with respect to the incoming wind.

In the stationary frame of reference, the sliders (c) were pushed and pulled by the guiding ring (b), performing a linear motion along the stationary hub (d) in the global Y-axis direction. Their movement determined the deformation of blades. In the initial state, the guide ring centre (e) and the rotor revolution axis (f) coincided. Thus, the blades were non-deformed and without pre-tension. During the first turbine revolution, the guiding

ring eccentricity gradually increased to achieve $m = 0.1$ m displacement (10% eccentricity shown in Fig. 4) and then remained constant for the rest of the simulations. The guiding ring rotated in the counter-clockwise direction around the rotor revolution axis along the trajectory indicated with red dashed circle in Fig. 4 with the angular velocity ω. The contacts of the sliders and the guiding ring as well as the sliders and the hub were defined as frictionless. Also, the blade tips freely rotated without friction around their anchoring axes at two sliders and the stationary hub. A similar type of symmetry condition as in the CFD module was applied due to the quasi-2D approach. Additionally, the centrifugal forces acting on the blades were introduced.

2.3 Coupling of fluid flow and structural solvers

In order to deform blades, the two-way FSI coupling method was applied. The corresponding regions at walls were indicated in the fluid flow and structural models. The blade deformation determined in the structural solver was transferred to the flow solver and the aerodynamic loads at walls were transferred back to the structural solver. Exchange of data between the solvers was carried out in an implicit way every five sub-iterations and at the end of each time step.

Blade deflection joined with specified rotation of the fluid flow overset meshes resulted in a complex motion of turbine rotor, resembling its real operation. A spring smoothing method was applied to avoid negative volumes of deformed cells in the overset meshes. It treated edges between any two nodes as a network of interconnected springs. Distances in an undeformed mesh constituted the equilibrium state. According to Hook's law, node displacements at blade boundaries generated proportional forces, which influenced the deformation of further mesh regions [16].

3 Results and discussion

Results obtained for all three types of computational models are presented in Table 1. Each time, at least 15 rotor revolutions were solved to obtain a fully developed flow. The torque (T) due to aerodynamic loads on the rotor blades was recorded at each time step. The coefficients of torque

$$C_t = \frac{4T}{\rho U^2 D^2 H} \tag{2}$$

and power

$$C_p = \mathrm{TSR} \cdot C_t = \frac{2T\omega}{\rho U^3 DH} \tag{3}$$

were calculated for the last five full revolutions and averaged to assess the turbine performance. The latter indicates machine efficiency.

For these three models, evaluation of discretization uncertainty was carried out using Richardson extrapolation, following the procedure presented in [24]. Three mesh sizes were generated for each case with blade edge sizes of 4 mm (fine mesh), 6 mm (medium mesh) and 8 mm (coarse mesh). The extrapolated value (RE), the apparent order of the method (P), the error ratio (R) and the fine-grid convergence index (FGCI) were determined for each approach. As presented in Table 1, changes in the performance parameters in every case were very low. Negative values of the error ratio (R) for two cases implied oscillatory convergence of the solution. Combined with very low differences between parameter values for the subsequent meshes, it caused that the apparent order of the method (P) in two cases significantly exceeded the order of equation discretization. The highest value of the numerical uncertainty in the fine-grid solutions was obtained for the overset approach with rigid blades (FGCI = 1.59%), whereas for the case of the rotor with deformable blades it was negligibly low. Therefore, the solutions of the fine meshes can be treated as mesh independent and their outcomes were further analysed and discussed.

Table 1: Mesh size dependence study of performed simulations.

	Sliding mesh, rigid blades			Overset mesh, rigid blades			Overset mesh, deformable blades		
	Fine	Medium	Coarse	Fine	Medium	Coarse	Fine	Medium	Coarse
Number of elements	316617	213639	152699	467684	285545	203388	467684	285545	203388
C_t	0.3111	0.3059	0.3063	0.3136	0.3171	0.3155	0.4866	0.4868	0.4882
C_p	0.2489	0.2447	0.2450	0.2508	0.2538	0.2524	0.3893	0.3894	0.3906
RE(C_t)	0.3117			0.3096			0.4866		
P	5.79			1.32			5.77		
R	-0.076			–0.460			6.466		
FGCI	0.24%			1.59%			$< 0.00\%$		

In order to assess the overset mesh model capabilities, its prediction of the performance of the rigid blade turbine was compared with the traditional

sliding mesh method. The torque and power coefficients ($C_t = 0.311$ and $C_p = 0.249$ for the sliding mesh method; $C_t = 0.314$ and $C_p = 0.251$ for the overset method) differed only by 0.8%. It confirmed that the overset mesh prediction was of the same quality as the sliding mesh approach typically used in Savonius turbine simulations. The obtained C_p values were about 20% higher than usually reported for such turbines [4, 25], but were in the range of values obtained when 2D simplification was applied [26, 27], where the influence of endplates is omitted.

Introduction of the blade deformation with 10% eccentricity provided the torque and power coefficients $C_t = 0.487$ and $C_p = 0.389$. They were 55% higher in comparison to the rigid blades turbine. This increase was in agreement with our previous investigations [7]. However, the obtained value of the power coefficient was slightly higher, probably due to the application of the blade overlap.

The changes of the power coefficients for the subsequent time steps in the last five rotor revolutions are presented in Figs. 5–7 for three cases under study. The sliding mesh approach for the turbine with rigid blades (Fig. 5) provided a negligible dispersion of calculated values, hence a smooth periodic curve for each considered revolution was observed. It was due to the fact that the data were transferred between two meshes in the stationary and rotational frame of reference through the constant interface with cells of comparable size at both sides. Results obtained from separate revolutions closely matched and all five curves nearly overlapped each other, which confirmed that a sufficient number of turbine revolutions was solved.

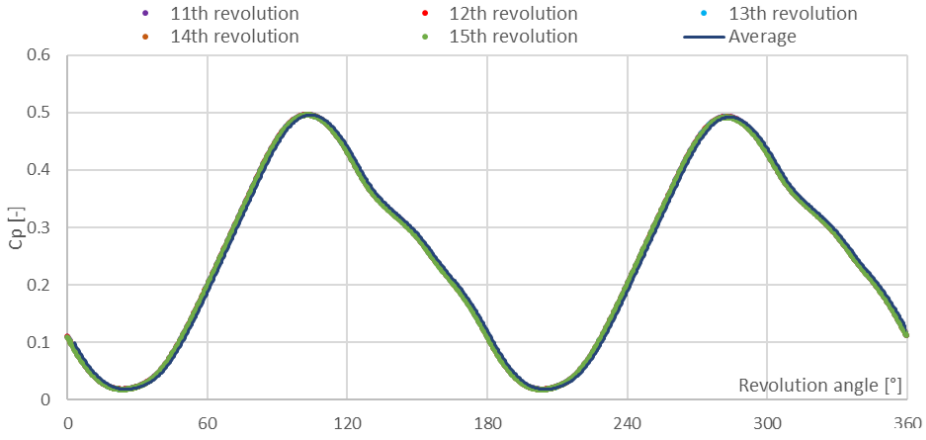

Figure 5: Power coefficient (C_p) for the rigid blade turbine, sliding mesh solution.

An additional curve presenting the coefficient values as a moving average of the subsequent ten time steps was introduced for additional visualisation. It overlaps with the remaining ones. The maximum value of the power coefficient approached 0.5 for revolution angles equal to about 105° and 285°, while the minimum value equal to about 0.02 corresponded to revolution angles of about 23° and 203°.

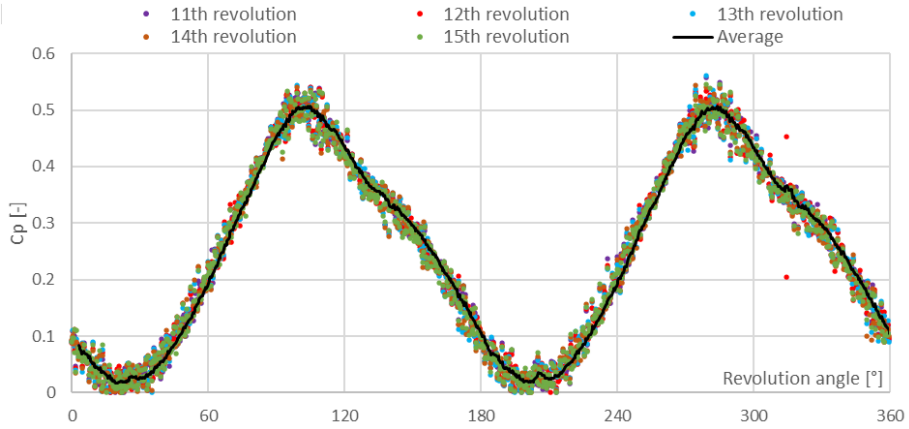

Figure 6: Power coefficient (C_p) for the rigid blade turbine, overset mesh solution.

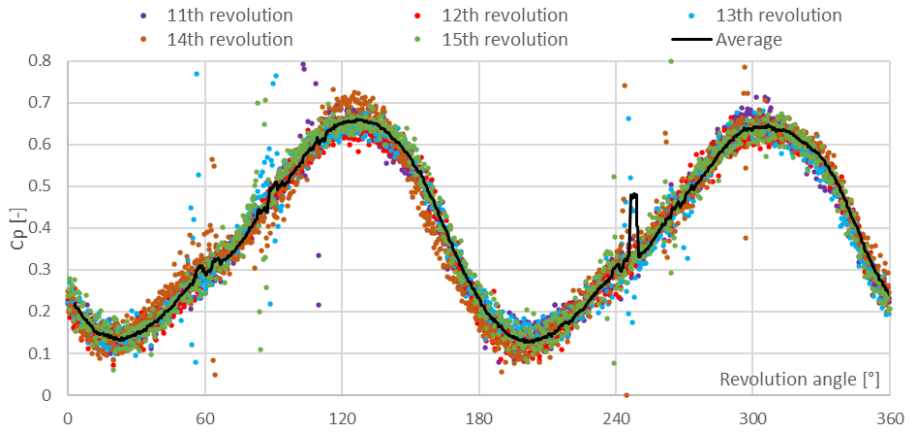

Figure 7: Power coefficient (C_p) for the deformable blade turbine, overset mesh solution.

In the case of the overset mesh approach, cells of the background and moving blade surroundings were merged and the solution variables were passed and interpolated between them in the subsequent time steps. Interpolation

errors caused a dispersion of calculated values as one can notice in Figs. 6 and 7. In the case of the rigid blade simulation, the dispersion was very limited. The significantly higher dispersion for the solution of the turbine with deformable blades resulted from additional interpolation errors due to mesh deformation. Nevertheless, the periodic changes of the power coefficient can be easily noticed in both cases and the averaged values of the coefficient for the last five rotor revolutions differed negligibly. The additional curves with the moving average of the coefficient in the subsequent ten time steps present the periodic changes with several artefacts related to the interpolation errors. The angles of the power coefficient maxima and minima for the rigid blade turbine corresponded precisely to the angles in the sliding mesh approach. In the case of the deformable blade turbine, the peak value exceeding 0.6 was reached for revolution angles of about 125° and 305°. The minimum value was achieved for similar revolution angles as in the previous cases.

Different computational power demands of the presented methods were observed. The investigation of the rigid blades turbine with the overset approach lasted about two times longer than with the sliding mesh method. The same scenario implemented for deformable blades turbine was the most demanding in terms of time and computational resources. Apart from the additional requirements of the fluid dynamics solver due to mesh deformation, the structural one was also involved and the solution data were synchronically exchanged between both. In this case, the calculation time was about five times longer.

4 Conclusions

The quasi-2D numerical model was developed to evaluate the aerodynamic performance of the Savonius wind turbine with the blades continuously deformed during rotation. It implemented the overset mesh approach, a predefined deformation mechanism and a two-way FSI coupling between the CFD and structural solvers. The mechanism was expected to raise a positive torque of the advancing blade and, at the same time, decrease the negative torque of the returning blade. The performance of the deformable blade turbine was compared with a conventional rigid Savonius turbine, simulated with the overset approach as well as the typical sliding mesh approach. All considered cases were solved with three grids to evaluate discretization uncertainty.

Below are the main outcomes of the described works.

- The sliding mesh and overset mesh models of the Savonius turbine with the rigid blades provided comparable results. Even though the interpolation errors in the overset method resulted in a dispersion of results in the subsequent time steps, the averaged values of the power coefficients differed only by 0.8%. Also, the coefficient changes during the turbine rotation were the same as for the sliding mesh method. Hence, the proposed overset mesh models can be treated as credible in the evaluation of Savonius wind turbines. Nevertheless, they require significantly longer computational time.

- The developed numerical model was successfully applied to the Savonius wind turbine with deformable blades. For the blade deformation magnitude defined by the rotation axis eccentricity equal to 10% of the rotor diameter, the power coefficient of 0.389 was reached. It was 55% higher than the rigid blades turbine with $C_p = 0.251$.

- The overset method applied to simulate the Savonius rotor with deformable blades simplified the complexity of the CFD model presented in [7]. The described approach omitted a need for complicated and time-consuming remeshing of the rotor neighbourhood domain, which might lead to simulation instabilities and failures. The overset mesh was deformed without a noticeable loss of quality, which limited the numerical problems, but the dispersion of results in the subsequent time steps due to interpolation errors was still observed.

The obtained results showed that the blade deformation of a Savonius wind turbine could significantly improve its efficiency. Therefore, it is a promising object for further research and optimisation.

Acknowledgement This paper was created as a part of a project "*Wdrożeniowa Szkoła Doktorancka*" (POWR.03.02.00-00-I042/16-00) co-financed by the European Union under the European Social Fund.

Received 9 September 2021

References

[1] Akwa J.V., Vielmo H.A., Petry A.P.: *A review on the performance of Savonius wind turbines*. Renew. Sust. Energ. Rev. **16**(2012), 5, 3054–3064.

[2] Masdari M., Tahani M., Naderi M.H., Babayan N.: *Optimization of airfoil Based Savonius wind turbine using coupled discrete vortex method and salp swarm algorithm*. J. Clean. Prod. **222**(2019), 47–56.

[3] Alom N., Saha U.K..: *Influence of blade profiles on Savonius rotor performance: Numerical simulation and experimental validation*. Energ. Convers. Manage. **186**(2019), 267–277.

[4] Zemamou M., Aggour M., Toumi A.: *Review of savonius wind turbine design and performance*. Energy Proced. **141**(2017), 383–388.

[5] Tartuferi M., D'Alessandro V., Montelpare S., Ricci R.: *Enhancement of savonius wind rotor aerodynamic performance: A computational study of new blade shapes and curtain systems*. Energy **79**(2015), 371–384.

[6] Mauro S., Brusca S., Lanzafame R., Messina M.: *CFD modeling of a ducted Savonius wind turbine for the evaluation of the blockage effects on rotor performance*. Renew. Energ. **141**(2019), 28–39.

[7] Sobczak K., Obidowski D., Reorowicz P., Marchewka E.: *Numerical investigations of the savonius turbine with deformable blades*. Energies **13**(2020), 14, 3717.

[8] Obidowski D., Sobczak K., Jozwik K., Reorowicz P.: Vertical Axis Wind Turbine with a Variable Geometry of Blades. European Patent Application 19199085.2, 24 Sept. 2019.

[9] Kamoji M.A., Kedare S.B., Prabhu S.V..: *Experimental investigations on single stage modified Savonius rotor*. Appl. Energ. **86**(2009), 7-8, 1064–1073.

[10] Lipian M., Czapski P., Obidowski D.: *Fluid-structure interaction numerical analysis of a small, urban wind turbine blade*. Energies **13**(2020), 7, 1–15.

[11] Marzec Ł., Buliński Z., Krysiński T.: *Fluid structure interaction analysis of the operating Savonius wind turbine*. Renew. Energ. **164**(2021), 272–284.

[12] Chan C.M., Bai H.L., He D.Q.: *Blade shape optimization of the Savonius wind turbine using a genetic algorithm*. Appl. Energ. **213**(2018), 148–157.

[13] Saeed H.A.H., Elmekawy A.M.N., Kassab S.Z.: *Numerical study of improving Savonius turbine power coefficient by various blade shapes*. Alexandria Eng. J. **58**(2019), 2, 429–441.

[14] Mohamed M.H., Janiga G., Pap E., Thčvenin D.: *Optimization of Savonius turbines using an obstacle shielding the returning blade*. Renew. Energ. **35**(2010), 11, 2618–2626.

[15] Kacprzak K., Liskiewicz G., Sobczak K.: *Numerical investigation of conventional and modified Savonius wind turbines*. Renew. Energ. **60**(2013), 578–585.

[16] ANSYS Inc.: *ANSYS Fluent 20.2 User's Guide*. ANSYS Inc., Canonsburg, 2020.

[17] ANSYS Inc.: https://www.ansys.com/. ANSYS Inc., Canonsburg, 2020.

[18] Menter F.R., Langtry R., Völker S, Huang P.G.: Transition modelling for general purpose CFD codes. In: Proc. ERCOFTAC Int. Symp. on Engineering Turbulence Modelling and Measurements 6; ETMM6, Sardinia, 23-25 May 2005, 31–48.

[19] Kerikous E., Thévenin D.: *Optimal shape of thick blades for a hydraulic Savonius turbine*. Renew. Energ. **134**(2019), 629–638.

[20] Ferrari G., Federici D., Schito P., Inzoli F., Mereu R.: *CFD study of Savonius wind turbine: 3D model validation and parametric analysis*. Renew. Energ. **105**(2017), 722–734.

[21] Kacprzak K., Sobczak K.: *Numerical analysis of the flow around the Bach-type Savonius wind turbine*. J. Phys. Conf. Ser. **530**(2014), 1, 012063.

[22] Sobczak K.: *Numerical investigations of an influence of the aspect ratio on the Savonius rotor performance*. J. Phys. Conf. Ser. **1101**(2018), 1, 012034.

[23] Krysiński T., Buliński Z., Nowak A.J.: *Numerical modeling and preliminary validation of drag-based vertical axis wind turbine*. Arch. Thermodyn. **36**(2015), 1, 19–38.

[24] Celik I.B., Ghia U., Roache P.J., Freitas C.J., Coleman H., Raad P.E.: *Procedure for estimation and reporting of uncertainty due to discretization in CFD applications*. J. Fluids Eng. **130**(2008), 7, 0780011–0780014.

[25] Akwa J.V., Vielmo H.A., Petry A.P.: *A review on the performance of Savonius wind turbines*. Renew. Sust. Energ. Rev. **16**(2012), 5, 3054–3064.

[26] D'AlessandroV., Montelpare S., Ricci R., Secchiaroli A.: *Unsteady aerodynamics of a Savonius wind rotor: A new computational approach for the simulation of energy performance*. Energy **35**(2010), 8, 3349–3363.

[27] Antar E., Elkhoury M.: *Casing optimization of a Savonius wind turbine*. Energ. Rep. **6**(2020), 184–189.